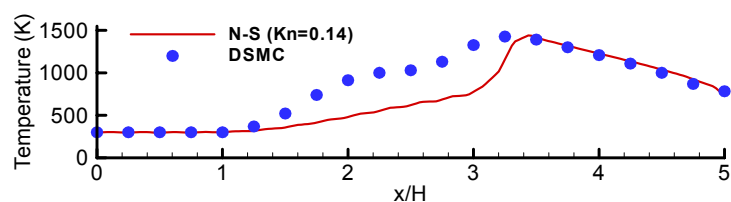
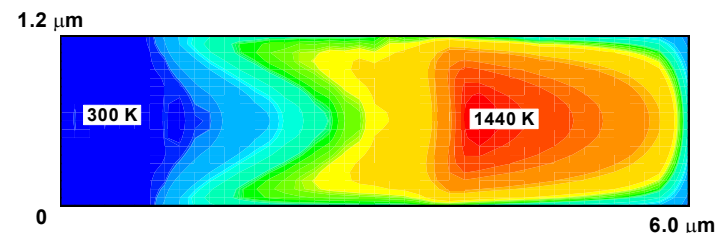


AIAA-2003-4051

# **Numerical Study of Heat Transfer in High Speed Microflows**

Reni Raju and Subrata Roy

Computational Plasma Dynamics Laboratory  
Kettering University  
Flint, MI 48504



**36th AIAA Thermophysics Conference**  
23 - 26 Jun 2003  
Orlando, Florida

## Numerical Study of Heat Transfer in High Speed Microflows

**Reni Raju<sup>\*</sup> and Subrata Roy<sup>†</sup>**  
*Computational Plasma Dynamics Laboratory  
Department of Mechanical Engineering  
Kettering University, Flint, Michigan 48504, USA*

Heat transfer characteristics in microchannels have been investigated using a finite element based hydrodynamic model with first order slip/jump boundary conditions. Results for high-speed gas flow for two separate cases for a microchannel with an aspect ratio of 5 have been compared with published DSMC results. Helium and nitrogen have been utilized as working fluid and the Knudsen number ranges from slip to transition regime. Presented results show that hydrodynamic model has excellent shock capturing capability for high speed micro flows.

### NOMENCLATURE

$C_p$	Specific heat at constant pressure
$\gamma$	Specific heat ratio
$\lambda$	Mean free path of the fluid
$k$	Thermal conductivity
$Kn$	Knudsen Number
$Ma_0$	Reference Mach number
$\mu$	Coefficient of viscosity
$Pr$	Prandtl number
$P$	Gas pressure
$P_0$	Reference pressure
$\rho$	Gas density
$\rho_0$	Reference density
$R$	Reduced gas constant
$\sigma_v$	Tangential-momentum-coefficient
$\sigma_T$	Thermal-momentum-coefficient
$t$	Time
$T$	Gas temperature
$T_0$	Reference temperature
$T_w$	Wall temperature
$u$	Gas velocity in $x$ -direction
$u_0$	Reference velocity
$u_w$	Gas velocity on the walls
$v$	Gas velocity in $y$ -direction

### INTRODUCTION

Advancements in micromachining techniques and potential areas of application have led to the significant development of the micro and meso-scale systems. Specifically, developments of micro-heaters, micro-heat exchangers/sinks for electronic cooling, microspacecraft controls and similar devices emphasize the need to comprehend the heat transfer characteristics of fluids in microchannels. Typically, mechanical devices with dimensions below 1 mm up to 1  $\mu\text{m}$  are called microelectromechanical systems (MEMS). At these scales however the dimensions of the system itself becomes comparable to the mean free path of the particles inside the system. For liquid, this in turn tends to make the flow granular in nature, while for gases the flow becomes rarefied. Since fundamentally the flow behavior and heat transfer characteristics in micro devices are different than in macro systems it is necessary to understand and analyze the physics/laws governing these systems. Studies reflect that the standard continuum approach of considering the bulk of the fluid with no-slip wall conditions can no longer predict the momentum and heat transfer accurately in microdevices. As

<sup>\*</sup> Graduate Student, Email: [raju8515@kettering.edu](mailto:raju8515@kettering.edu), Student member, AIAA.

<sup>†</sup> Associate Professor, Email: [sroy@kettering.edu](mailto:sroy@kettering.edu), Associate Fellow, AIAA.

Copyright © 2003 by the authors. Published by the American Institute of Aeronautics and Astronautics, Inc. with permission.

the flow becomes molecular a number of other parameters start playing significant role in governing the heat and momentum transfer. These include the surface forces, roughness, rarefaction, viscous forces and thermal creep<sup>1</sup>, which are not dominant in macroscopic flows.

The degree of rarefaction and applicability of the continuum model is determined by the local value of the Knudsen number and is defined as  $\text{Kn} = \lambda/\Lambda = 16\mu/5\rho\sqrt{2\pi RT}$  (based on Chapman-Enskog result), where  $\lambda$  is the mean free path of the fluid and  $\Lambda$  is the characteristic dimension of the system. Depending on the value of Knudsen number the flow can be divided into four categories.<sup>2</sup> For  $\text{Kn} < 0.001$ , the flow can be assumed to be a continuum such is the case for macroscopic flows, while for  $\text{Kn} > 10$  it becomes free-molecular. However, in the region of  $0.001 - 10$  the flow is neither sufficiently continuum nor completely molecular. Thus, it can be further divided into two separate regions, slip-flow regime for  $0.001 < \text{Kn} < 0.1$  and transition regime for  $0.1 < \text{Kn} < 10$ .

It has been found that the Navier-Stokes equations<sup>4</sup> with first order velocity-slip<sup>3</sup> and temperature-jump<sup>4</sup> boundary correction works well for the slip flow regime ( $0.001 < \text{Kn} < 0.1$ ). However, with the increasing  $\text{Kn}$  the bulk nature of the fluid properties reduces and the flow becomes molecular. Due to the rarefaction of the fluids higher order boundary conditions are suggested<sup>1</sup> when the flow enters the transition regime ( $0.1 < \text{Kn} < 10$ ). The general computational tools for this region are Boltzmann equation methods, statistical methods, and Burnett equation with slip boundary conditions.<sup>5</sup>

Over the past two decades several experimental investigations have been carried out to determine the heat transfer characteristics in microchannels. In one of the earliest experiments Wu & Little<sup>6</sup> have measured heat transfer in fine channels. Pfahler *et al.*<sup>7</sup> have measured friction coefficients for laminar fluids in the microchannels. Choi *et al.*<sup>8</sup> have studied heat transfer in 3-81  $\mu\text{m}$  long microtubes. Heat transfer performance and cooling characteristics of sub-cooled liquid through 0.7mm deep microchannels have been measured by Peng *et al.*<sup>9</sup>. Adams *et al.*<sup>10</sup> have tried to enhance heat transfer of forced liquid convection using dissolved non-condensables while Mala *et al.*<sup>11</sup> investigated the effect of electric double layer in a flow between parallel plates.

The popular methods for analyzing the heat transfer characteristics of gases in microchannels include the particulate method of Boltzmann equation, direct simulation Monte Carlo<sup>12</sup> (DSMC) and Burnett equation models<sup>13,14</sup> since they give a better resolution for gas to surface interactions. Several investigators have used the DSMC approach especially in case of high-speed flows where the  $\text{Kn}$  is relatively high.<sup>5,15-17</sup> However the major drawback of this approach is that it is prohibitively expensive due to the high computation cost and time requirement<sup>1,15,18</sup> to achieve any practical resolution. The primary aim of microfluidics is to know the averaged quantities of the various parameters rather than the molecular information to predict the flow behavior. A more feasible approach would be considering bulk approach for the fluid flow while accommodating the different effects encountered in microfluidics like wall-slip, compressibility, rarefaction and thermal creep, thus yielding a closer approximation to the overall behavior of the flow in the domain at lower cost and practical turn around time.

A two dimensional hydrodynamic model based on the finite element method has been developed at Computational Plasma Dynamics Laboratory (CPDL) for investigating micro and meso-scale flows.<sup>19,20</sup> The first order slip/jump boundary conditions utilized in this model has predicted subsonic gas flow through microthruster<sup>19</sup> and benchmarked both experimental<sup>21</sup> and numerical<sup>22</sup> results for a microchannel and nanopore<sup>20</sup>. As a complement to our recent publication<sup>20</sup>, this paper aims to extend the applicability of hydrodynamic model to investigate heat transfer characteristics of high-speed flows through microchannels having a Knudsen number range of 0.062 – 0.14. The study is restricted to the gas flows. The results have been compared to the DSMC results of Oh *et al.*<sup>15</sup> and Liou *et al.*<sup>16</sup>.

## **PROBLEM DESCRIPTION**

The two-dimensional microchannel model shown in Figure 1 is an extension of the experimental setup of Pong *et al.*<sup>21</sup> used to study Poiseuille flow through long microchannels. The end effects have been neglected for the two dimensional analysis. The channel geometry have been modified by Oh *et al.*<sup>15</sup> for working fluid helium to an aspect ratio (L/H) of 5, in order to obtain hypersonic flow conditions. The value of Knudsen number is 0.14 for this case. The second case presented by Liou

et al.<sup>16</sup> is similar to the first in terms of dimensions. However the working fluid is nitrogen for this case giving a lower Knudsen number of 0.062. The microchannel dimensions and flow parameters are enlisted in the Table 1. The flow is simulated at near atmospheric conditions. A free stream region **B** is specified near the inlet section of the microchannel where the free gas flow takes place. The boundary conditions remain the same for the two cases.

	Case 1	Case 2
<b>Fluid</b>	Helium	Nitrogen
<b>L (μm)</b>	6.0	6.0
<b>H (μm)</b>	1.2	1.2
<b>B (μm)</b>	1.0	0.6
<b>Kn</b>	0.14	0.062
<b>T<sub>0</sub> (K)</b>	298	300
<b>T<sub>w</sub> (K)</b>	298	323
<b>Ma<sub>0</sub></b>	5.0	4.15
<b>P<sub>0</sub> (Pa)</b>	1.01 x 10 <sup>5</sup>	1.01 x 10 <sup>5</sup>
<b>R (J/kg.K)</b>	2076.9	296.8
<b>C<sub>p</sub>(J/kg.K)</b>	5192.6	1039.0
<b>μ (N-s/m<sup>2</sup>)</b>	2.066 x 10 <sup>-5</sup>	1.85 x 10 <sup>-5</sup>
<b>k (W/k.m)</b>	0.152	0.0259
<b>γ</b>	1.667	1.40

Table 1: Model dimensions and flow parameters

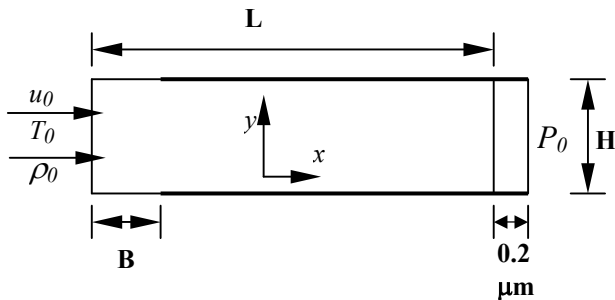


Figure 1: Schematic of microchannel geometry.<sup>15</sup>

The standard two-dimensional, time-dependent, compressible Navier-Stokes (NS) form with constant viscosity is used to analyze the gas flow through microchannels,

#### Conservation of Mass:

$$\frac{\partial \rho}{\partial t} + \frac{\partial \rho u}{\partial x} + \frac{\partial \rho v}{\partial y} = 0 \quad (1)$$

#### Conservation of x- momentum:

$$\frac{\partial \rho u}{\partial t} + u \frac{\partial \rho u}{\partial x} + v \frac{\partial \rho u}{\partial y} + \frac{\partial P}{\partial x} - \mu \left( \frac{\partial^2 u}{\partial x^2} + \frac{\partial^2 u}{\partial y^2} + \frac{1}{3} \left( \frac{\partial^2 u}{\partial x^2} + \frac{\partial^2 v}{\partial x \partial y} \right) \right) = 0 \quad (2)$$

#### Conservation of y- momentum:

$$\frac{\partial \rho v}{\partial t} + u \frac{\partial \rho v}{\partial x} + v \frac{\partial \rho v}{\partial y} + \frac{\partial P}{\partial y} - \mu \left( \frac{\partial^2 v}{\partial x^2} + \frac{\partial^2 v}{\partial y^2} + \frac{1}{3} \left( \frac{\partial^2 v}{\partial y^2} + \frac{\partial^2 u}{\partial x \partial y} \right) \right) = 0 \quad (3)$$

#### Conservation of energy:

$$\rho C_p \frac{DT}{Dt} - \frac{DP}{Dt} - \frac{\partial}{\partial x} \left( k \frac{\partial T}{\partial x} \right) - \frac{\partial}{\partial y} \left( k \frac{\partial T}{\partial y} \right) - \mu \left( 2 \left( \frac{\partial u}{\partial x} \right)^2 + 2 \left( \frac{\partial v}{\partial y} \right)^2 + \left( \frac{\partial v}{\partial x} + \frac{\partial u}{\partial y} \right)^2 - \frac{2}{3} \left( \frac{\partial u}{\partial x} + \frac{\partial v}{\partial y} \right)^2 \right) = 0 \quad (4)$$

The Pressure is defined using the perfect Gas law,

$$P = \rho RT \quad (5)$$

The “no-slip” wall condition is defined as having all components of the velocity vanish at the solid wall. However, as the macroscopic length scale becomes comparable to the fluid mean free path, this description becomes vague and the walls “move”. At this stage, streaming velocity at the wall can be described comprising of the streaming velocity of incident particles and that of the scattered particles. Maxwell<sup>3</sup> derived slip relations for dilute, monoatomic gases which have been implemented in the momentum equation,

$$u_g - u_w = \frac{2 - \sigma_V}{\sigma_V} \lambda \left( \frac{\partial u}{\partial y} \right)_w + \frac{3}{4} \frac{\mu}{\rho T_g} \left( \frac{\partial T}{\partial x} \right)_w \quad (6a)$$

Eqn. (6a) can be modified to the following form using the definition of Kn,

$$-\mu \left( \frac{\partial u}{\partial y} \right)_w = \frac{5 \rho \sigma_V \sqrt{2 \pi R T}}{16 (2 - \sigma_V)} \left( u_w - u_g + \frac{3}{4} \frac{\mu}{\rho T_g} \left( \frac{\partial T}{\partial x} \right)_w \right) \quad (6b)$$

Corresponding temperature-jump relation for the energy equation was derived by von Smoluchowski<sup>4</sup> as

$$T_g - T_w = \frac{2 - \sigma_T}{\sigma_T} \left[ \frac{2\gamma}{\gamma + 1} \right] \frac{\lambda}{\text{Pr}} \left( \frac{\partial T}{\partial y} \right)_w \quad (7a)$$

Eqn. (7a) can also be modified similarly,

$$-k \left( \frac{\partial T}{\partial y} \right)_w = \frac{\sigma_T \sqrt{2\pi RT}}{2 - \sigma_T} \left[ \frac{\gamma + 1}{2\gamma} \right] \frac{5\rho C_p}{16} (T_w - T_g) \quad (7b)$$

In eqns. (6)-(7),  $u_g$  and  $T_g$  are the velocity and temperature of the gas adjacent to the wall, while  $u_w$  and  $T_w$  are the velocity and temperature at the wall. The tangential-momentum accommodation coefficient,  $\sigma_v$  and the thermal accommodation coefficient,  $\sigma_T$  at the walls indicate the molecular fraction reflected diffusively from the walls. The second term in the eqn. (6a) is known as thermal creep, which generates slip velocity in the direction opposite to the increasing temperature.

Traditionally, the first order equations (6)-(7) are applied as long as  $\text{Kn} < 0.1$ . Karniadakis and Beskok<sup>1</sup> have presented a higher order slip boundary condition, which is second order accurate, for predicting flow accurately for higher Knudsen number in the transition regime. It has been suggested that Maxwell's first order boundary condition breaks down near  $\text{Kn} = 0.15$  (Sreekanth<sup>23</sup>, Piekos and Breuer<sup>24</sup>). However, Roy *et al.*<sup>20</sup> have successfully utilized the first-order boundary condition for higher Knudsen number of up to 7.36 and it has also been suggested that the higher order slip boundary conditions may actually deviate from the actual solution more than the first order Maxwell's wall-slip conditions<sup>3</sup>. Due to these reasons, we would restrict slip to first order conditions (6)-(7).

## NUMERICAL METHOD

The system of eqns. (1-5) can be represented in more concise form as

$$L(\mathbf{q}) = \frac{\partial \mathbf{q}}{\partial t} + \frac{\partial (\mathbf{f}_j - \mathbf{f}_j^v)}{\partial x_j} - \mathbf{s} = 0, \quad 1 \leq j \leq 2 \quad (8a)$$

$$\mathbf{q} = \begin{pmatrix} \rho \\ \rho u_i \\ \rho C_p T + P \\ 0 \end{pmatrix}, \quad \mathbf{f}_j = \begin{pmatrix} \rho u_j \\ u_j \rho u_i + P \delta_{ij} \\ u_j (\rho C_p T + P) \\ 0 \end{pmatrix}, \quad (8b)$$

$$\mathbf{f}_j^v = \begin{pmatrix} 0 \\ \tau'_{ij} \\ k \frac{\partial T}{\partial x_j} + \tau'_{ij} u_i \\ 0 \end{pmatrix}, \quad \mathbf{s} = \begin{pmatrix} 0 \\ 0 \\ 0 \\ P - \rho RT \end{pmatrix}, \quad 1 \leq i \leq 2$$

where  $\mathbf{q}$  is the state variable,  $\mathbf{f}$  is the kinetic flux vector,  $\mathbf{f}^v$  the dissipative flux vector and  $\mathbf{s}$  is the source term; and

$$\tau'_{ij} = \mu \left( \frac{\partial u_i}{\partial x_j} + \frac{\partial u_j}{\partial x_i} \right) + \delta_{ij} \lambda \frac{\partial u_k}{\partial x_k}, \quad 1 \leq i, j, k \leq 2.$$

The difficulty involved in achieving a steady state solution for eqns. (8a-b) directly is due to the selection of initial conditions. The conventional method of achieving a steady state solution is to use the time term as a relaxation parameter in the equation system and run the problem till the transient features die down. Here we utilize an artificial diffusion term as an initial condition generator to obtain a final steady state solution.

Eqn. (8) can be modified in the following steady state form,

$$L(\mathbf{q}) = \frac{\partial (\mathbf{f}_j - \mathbf{f}_j^v)}{\partial x_j} - \beta \frac{\partial^2 \tilde{\mathbf{q}}}{\partial x_j^2} - \mathbf{s} = 0, \quad 1 \leq j \leq 2 \quad (9)$$

where,  $\tilde{\mathbf{q}}^T = (0, u_i, T, 0)$  and  $\beta$  is a diffusion perturbation parameter that can be varied separately for each state variable. As  $\beta \rightarrow 0$ , eqn. (9) reverts back to steady state form of equation (8). Initially  $\beta$  is set to a sufficiently high value so as to generate a diffused but stable convergence to steady state solution. Progressive reduction of  $\beta$  is carried out till the final steady state solution with  $\beta \rightarrow 0$  is achieved. This procedure is analogous to using the transient relaxation.

Using any admissible test function  $w$ , the variational integral yields the *weak statement* (WS) for equation (9). Thereafter, the domain  $\Omega$  and integrated variables  $\mathbf{q}$  are spatially discretised ( $\Omega_e$  and  $\mathbf{Q}$ ) using Lagrange basis functions  $N_k$  complete to the degree  $k$ .

$$WS = \int_{\Omega} w L(\mathbf{q}) d\Omega = 0, \Rightarrow WS^h = S_e \left( \int_{\Omega_e} N_k L_e(\mathbf{Q}) d\tau \right) = 0 \quad (10a)$$

$$WS^h = S_e \left( \int_{\Omega_e} N_k (-s) d\tau - \int_{\Omega_e} \frac{\partial N_k}{\partial x_j} (\mathbf{f}_j - \mathbf{f}_j^v)_e d\tau + \oint_{\partial\Omega_e \cap \partial\Omega^h} N_k (\mathbf{f}_j - \mathbf{f}_j^v)_e \hat{n}_j d\sigma \right) \quad (10b)$$

In (10), the superscript  $h$  denotes discretization and  $S_e$  symbolizes the "assembly operator" carrying local (element  $e$ ) matrix coefficients into the global arrays. The weak statement naturally yields the surface integrals via application of

Green-Gauss theorem in equation (10), which contains the unknown boundary fluxes wherever Dirichlet (fixed) boundary conditions are enforced. The zero gradient boundary conditions are automatically enforced via removal of the surface integral. For the slip flow boundary, appropriate surface integrals are replaced by incorporating the eqns. (6b) and (7b) into the momentum and energy equations. Independent of the physical dimension of  $\Omega$ , and for general forms of the flux vectors, the semi-discretized weak statement of equation (10) always yields an ordinary differential equation (ODE) system. The terminal ODE is then solved using a Newton-Raphson iterative scheme.

The computational channel geometry is discretized using two-dimensional non-overlapping 9-noded biquadratic finite elements. The continuity and equation of state are solved for density and pressure respectively using the four corner nodes of the element. For velocity and temperature calculations, all nine nodes of the biquadratic element are used.

#### Boundary Conditions

The inlet boundary conditions are fixed for velocity  $u_0$  (based on Mach number), temperature  $T_0$  and the density  $\rho_0$  (based on corresponding inlet pressure,  $P_0$ ) as listed in Table 1. The wall temperatures for both the top and bottom surfaces are set to be  $T_w$ . The velocity flux is  $\partial u / \partial x = 0$  at the outlet and the  $y$ -component of the velocity  $v=0$  is specified at the inlet. A backpressure equal to the inlet boundary pressure,  $P_0$  is specified at the outlet. The drawback faced for this problem is that outflow boundary conditions could not be replicated since the exact location of the outlet pressure is not clear in any of the references<sup>15,16</sup>. As a result we specify a backpressure  $P_0 = 1.01 \times 10^5$  Pa, 0.2  $\mu\text{m}$  downstream from the exit.

Near the entrance at the wall boundary for the length  $B$  ("lighter wall"), the accommodation coefficients are specified as  $\sigma_v = \sigma_T = 0.0$ , implying a specular reflection where only the tangential component of velocity of the impinging molecules is conserved; this is the freestream region. In the rest of the domain ("darkened wall") completely diffuse the gas to wall interactions is set with  $\sigma_v = \sigma_T = 1.0$  implying the gas molecules undergo a complete change in momentum after collision.

## RESULTS AND DISCUSSIONS

A single computational grid used for both cases consisting of 560 finite elements and 3485 nodes. Even though for a channel having an aspect ratio of 2500 with only a 1369 node grid was used earlier<sup>20</sup>, here a finer mesh is utilized for capturing better resolution of the high speed flow characteristics. In order to keep the consistency with the numerical report the length in x-direction is considered for the length mentioned in Table 1 ignoring the extra length of 0.2  $\mu\text{m}$  for both the cases. Case 1 would be referred to as for  $\text{Kn}=0.14$  and the latter as for  $\text{Kn}=0.062$  henceforth.

For  $\text{Kn} = 0.062$  the Mach number contours shows that the shock emerging from the walls move towards the center of the channel causing a distortion just ahead of the freestream section. The drop in the Mach number is smooth along the channel as is seen in figure 2(a). However, for the  $\text{Kn} = 0.14$  the contours in figure 2(b) plot a relatively sharper drop in velocity. This shows the prevailing viscous effects in the higher Knudsen number cases.

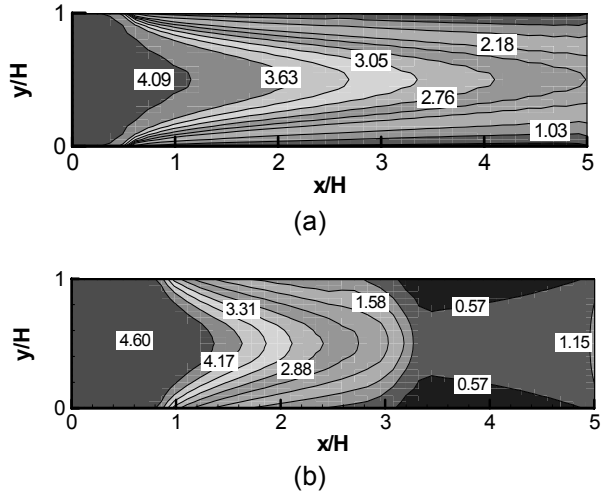


Figure 2. Mach number contours for (a)  $\text{Kn}=0.062$  and (b)  $\text{Kn} = 0.14$ .

The temperature contours for the two cases are shown in figure 3. Due to shock the thermal boundary is not completely developed for  $\text{Kn} = 0.062$ . The rise in the temperature is seen the downstream region near the exit, figure 3(a) at nearly  $x/H=4.2$ . This temperature jump is documented upstream for  $\text{Kn}=0.14$  at nearly  $x/H=3.4$  due to the increase in thermal boundary layer as shown in figure 3(b).

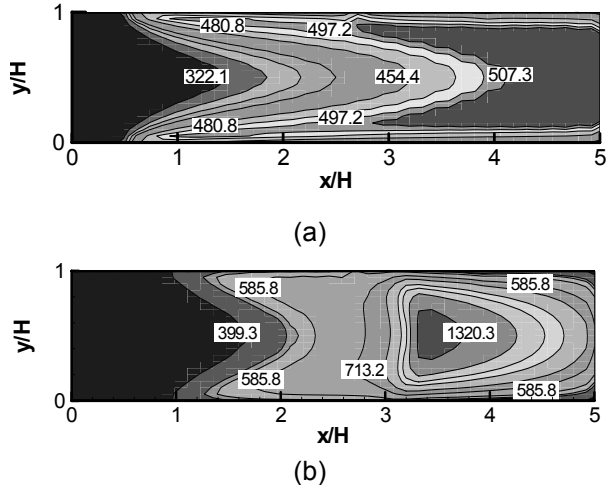


Figure 3. Temperature contours for (a)  $\text{Kn}=0.062$  and (b)  $\text{Kn} = 0.14$ .

The Mach number distribution along the centerline and near wall section of the flow in the streamwise direction is plotted for both the cases in Figure 4(a)-(b). These results are compared with reported DSMC solution<sup>15</sup> for  $\text{Kn}=0.14$ . The centerline Mach number for  $\text{Kn}=0.14$  shows a good comparison in the upstream and downstream region with DSMC results. In the mid-region, the observed deviation could be due to the difference in the specification of the location of back pressure as described before. The near wall distribution in figure 4(b) also shows a similar comparison with even exaggerated effect of the back pressure.

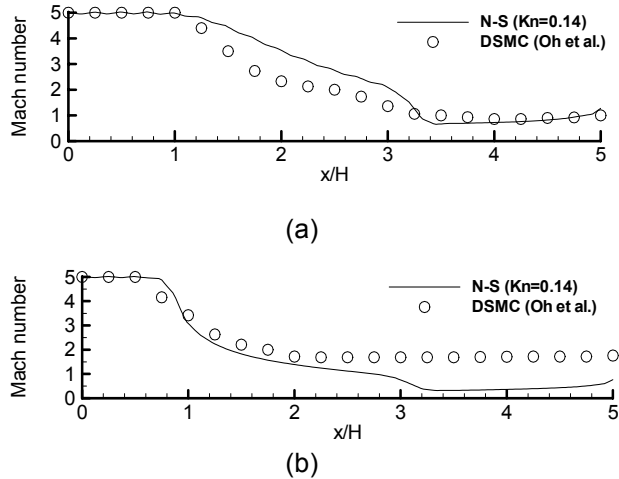


Figure 4. Comparison of, (a) centerline and (b) near wall, Mach number distribution of both N-S solutions with available DSMC results<sup>15</sup> for  $\text{Kn} = 0.14$ .

Figure 5 compares the centerline and near wall Mach number distribution for  $\text{Kn} = 0.062$ . Plotted solution in figure 5(a) shows a smoother drop in the Mach number along the channel centerline as compared to the  $\text{Kn} = 0.14$ , figure 4(a). The solution near the walls of the microchannel plotted in figure 5(b) shows that Mach number undergoes a drop immediately after the freestream region and there after nearly remains steady. Since no such data at this Knudsen number is not reported elsewhere there is no means for direct comparison with the literature.

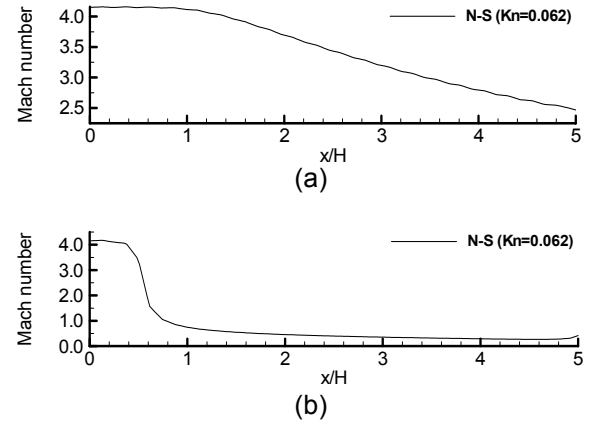


Figure 5. Mach number distribution of  $\text{Kn} = 0.062$  case, (a) at the centerline and (b) near the wall.

The centerline distribution of temperature for the two cases has been compared in figures 6(a)-(b). For  $\text{Kn} = 0.062$ , the temperature distributions are similar with a maximum difference of 100 K in the peak value prediction. For  $\text{Kn}=0.14$ , temperature profiles match in upstream and downstream region like the Mach number. The peak for the temperature matches closely with the referred data. However, compared to the DSMC result, the shock is sharper in the hydrodynamic solution.

Figure 7(a) shows the near wall temperature distribution for  $\text{Kn} = 0.062$  where the peak values of the N-S simulation differ from the DSMC results at the end of freestream region; however for the rest of the domain the values match closely. The solution plotted in figure 7(b) for  $\text{Kn}=0.14$  shows that the temperature near the walls remains below 600 K at all places. Deviation from published DSMC results is observed in the region from  $x/\text{H} = 0.8$  to 2.2. However similar deviation in temperature distribution was also documented for low (0.07) Knudsen number.<sup>14</sup>

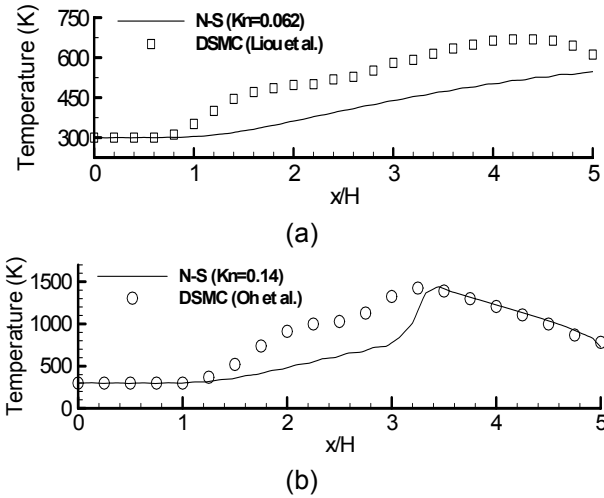


Figure 6. Comparison of centerline distribution of temperature compared with the available DSMC results for (a)  $Kn = 0.062$ <sup>16</sup> and (b)  $Kn = 0.14$ <sup>15</sup>.

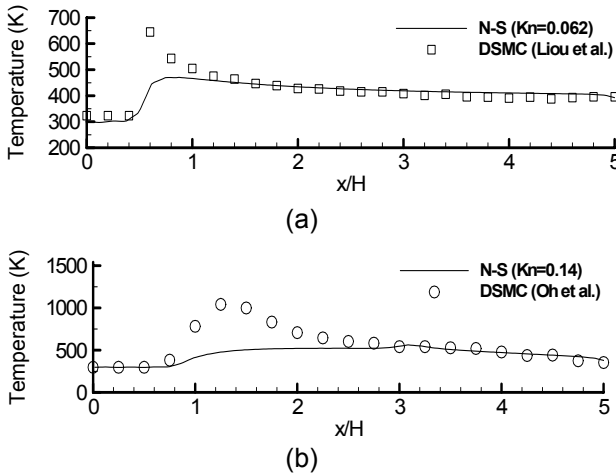


Figure 7. Comparison of near wall distribution of temperature compared with the available DSMC results for (a)  $Kn = 0.062$ <sup>16</sup> and (b)  $Kn = 0.14$ <sup>15</sup>.

Figure 8(a) shows the distribution of the Mach number for various crosswise sections taken along the length of the microchannel for  $x/H = 0.8, 1.6, 2.4, 3.2$  and  $4.0$ . For  $Kn = 0.14$  at  $x/H=0.8$ , the flow is in the freestream region and hence the profile is linear. This becomes parabolic for  $x/H=1.6$  and as the flow progresses downstream the Mach number profile the peak value decreases corresponding to the drop in velocity downstream. On the other hand, very small change in the parabolic profile for  $Kn = 0.062$  is noticeable in the downstream region. Evidently, higher Mach number produces more slip on the walls.

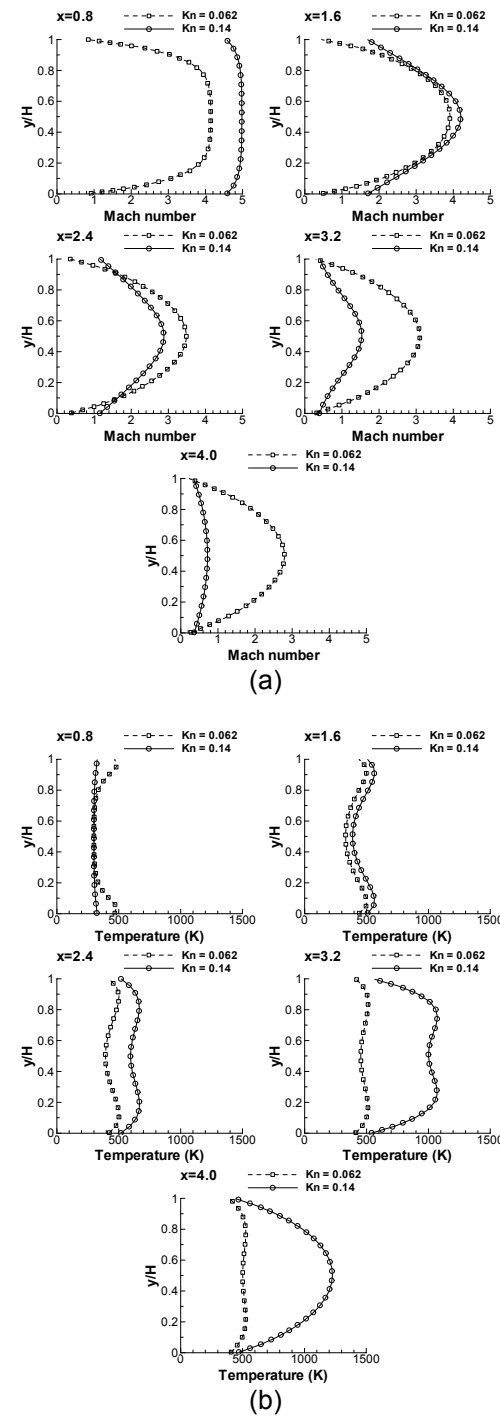


Figure 7. Comparison along the  $y$ -direction for various cross sections for  $Kn = 0.062$  and  $Kn = 0.14$  along the streamwise direction for; (a) Mach number and (b) Temperature.

Corresponding sections for the temperature distribution show the development of thermal boundary layer. Figure 8(b) depicts these

crosswise profiles of the temperature. In the freestream region the temperature remains linear. For  $Kn = 0.14$ , thermal boundary formation starts at  $x/H=0.8$  with knees near the top and bottom surfaces. This distortion merges towards the center of the channel as the flow develops. Finally at  $x/H= 4.0$  the flow becomes fully developed with both peaks vanishing. For  $Kn = 0.062$ , the development of the thermal boundary does not complete at  $x/H = 4.0$ . The contours in figure 3(a) show that the boundary formation continues beyond  $x/H = 4.2$ .

## CONCLUSIONS

A two-dimensional finite element based hydrodynamic model using the first order slip/jump boundary conditions has been utilized to simulate high-speed gas flows through short microchannels. The two cases considered incorporate different fluids, namely, helium and nitrogen. The higher Knudsen number case with helium reflects a higher heat transfer characteristics. The heat transfer characteristics predicted by the hydrodynamic model for this microchannel compared favorably with the reported DSMC results. The deviation in values could possibly be due to difference in location where the exit backpressure was specified.

## REFERENCES

<sup>1</sup>Karniadakis, G. and Beskok, A., 2002, "Micro Flows-Fundamentals and Simulation" Springer-Verlag New York, Inc.

<sup>2</sup>Schaaf, S.A. and Chambre, P.L., 1961, "Flow of rarefied gases," Princeton University Press, Princeton, New Jersey.

<sup>3</sup>Maxwell,J.C., 1879, "On stresses in rarefied gases arising from inequalities of temperature" *Philosophical Transactions of the Royal Society Part 1*, vol.170, pp.231-256.

<sup>4</sup>Smoluchowski, von M., 1898, "Ueber wärmeleitung in verdünnten gasen" *Annalen der Physik und Chemi*, vol. 64, pp. 101-30.

<sup>5</sup>Oran, E.S., Oh, C.K. and Cybyk, B.Z., 1998, "Direct simulation Monte Carlo: Recent advances and applications," *Annu. Rev. Fluid Mechanics*, vol. 30, pp. 403-441.

<sup>6</sup>Wu, P.Y. and Little, W.A., 1984, " Measurement of the heat transfer characteristics of gas flow in fine channel heat exchanger used for microminiature refrigerators," *Cryogenics*, vol. 24, pp. 415-423.

<sup>7</sup>Pfahler, J., Bau, H. and Zemel, J.N., 1990, "Liquid transport in micron and submicron channels," *Sensors and Actuators*, vol. A21-23, pp. 431-434.

<sup>8</sup>Choi, S.B., Barron, R.F. and Warrington, 1991," Fluid flow and heat transfer in microtubes," *Proc. ASME, DSC*-vol. 32, pp. 123-134.

<sup>9</sup>Peng X.F, Wang B.X., Peterson G.P and Ma, H.B, 1995, "Experimental Investigation of heat transfer in flat plates with rectangular microchannels", *International J. Heat Mass Transfer*, vol.38, no.1, pp.127-137.

<sup>10</sup>Adams, T.M., Ghiaasiann, S.M. and Abdel-Khalik, S.I., 1999, "Enhancement of liquid forced convection heat transfer in microchannels due to the release of dissolved noncondensables", *International J. Heat Mass Transfer*, vol.42, pp.3563-3573.

<sup>11</sup>Mala, G.M, Li, D. and Dale,J.D., 1997, " Heat Transfer and fluid flow in microchannels", *Int. Journal Heat and Mass Transfer*, vol.40, pp.3079-3088.

<sup>12</sup>Bird, G.A., 1994, "Molecular Gas Dynamics and the Direct Simulation of Gas Flows", Oxford, U.K., Oxford Science.

<sup>13</sup>Xue, H., Ji, H.M. and Shu, C., 2001, "Analysis of micro-Couette flow using the Burnett equations," *Int. Journal of Heat and Mass Transfer*, vol. 44, pp. 4139-4146.

<sup>14</sup>Agarwal R.K., Yun, K.Y. and Balakrishnan, R., 2001, "Beyond Navier-Stokes: Burnett equations for flows in contunnum-transition regime" *Physics of Fluids*, vol. 13, no. 10, pp. 3061-3085.

<sup>15</sup>Oh C.K., Oran E.S. and Sankovits R.S., 1997, "Computations of high speed, high Knudsen number microchannel flows", *Journal of Thermophysics & Heat Transfer*, vol. 11, pp. 497.

<sup>16</sup>Liou, W.W and Fang, Y., 2001, "Heat Transfer in Microchannel devices using DSMC", *Journal of Microelectromechanical Systems*, vol.10, no.2, pp.274-279.

<sup>17</sup>Mavriplis, C., Ahn, J.C. and Goulard, R., 1997, "Heat Transfer and flowfields in Short Microchannels using Direct Simulation Monte Carlo," *J. of Thermophysics and Heat Transfer*, vol. 11, no. 4, pp. 489-496.

<sup>18</sup>Gad-ek-hak, M., 1999, "The Fluid Mechanics of Microdevices- The Freeman Scholar Lecture" *Journal of Fluids Engineering*, vol.121, pp. 5-33.

<sup>19</sup>Raju ,R., Pandey, B.P. and Roy S., 2002, "Finite Element Model of Fluid Flow inside a Micro-Thruster", *NanoTech 2002 - "At the Edge of Revolution"*, Houston, Texas, AIAA-2002-5733.

<sup>20</sup>Roy, S., Raju, R., Chuang, H., Cruden, B. and Meyyappan, M., 2003, "Modeling gas flow through microchannels and nanopores," *Journal of Applied Physics*, vol.93, no.8, pp. 4870-79, 2003.

<sup>21</sup>Pong, K.C., Ho, C., Liu, J. and Tai, Y., 1994, "Non-Linear Pressure Distribution in Uniform Microchannels" *Application of Microfabrication to Fluid Mechanics*, FED –vol. 197, pp.51-56.

<sup>22</sup>Chen, C.S., Lee, S.M. and Sheu J.D., 1998, "Numerical Analysis of Gas flow in Microchannels." *Numerical Heat Transfer, Part A*, vol. 33, pp.749-762.

<sup>23</sup>Sreekanth, A.K., 1969, "Slip Flow through Long Circular Tubes", *Rarefied Gas Dynamics*, eds. Trilling, L. and Wachman, H. Y., Academic Press, New York , vol. 1, pp. 667-680.

<sup>24</sup>Piekos, E. & Breuer, K., 1995, "DSMC modeling of microchannel devices," *AIAA Thermophysics Conference, San Diego, CA*, AIAA 95-2089.

<sup>25</sup>Lockerby, D.A. and Reese, J.M., 2003, "High resolution Burnett simulations of micro Couette flow and Heat Transfer," *Journal of Computational Physics*, (article in press).